Experimental characterization of the AA7075 aluminum alloy using hot shear compression test

Trunal Bhujangrao[1,2,*], Fernando Veiga[1], Catherine Froustey[3], Sandra Guérard[3], Edurne Iriondo[2], Philippe Darnis[3], Franck Girot Mata[2,4]

[1]*TECNALIA, Basque Research and Technology Alliance (BRTA), Parque Científico y Tecnológico de Gipuzkoa, 20009 Donostia-San Sebastián, Spain*

[2]*Department of Mechanical Engineering, University of the Basque Country (UPV/EHU), 48013 Bilbao, Spain*

[3]*Univ. Bordeaux, I2M -DuMAS, UMR 5295, CNRS, F-33400 Talence, France*

[4]*IKERBASQUE, Basque Foundation for Science, 48013 Bilbao, Spain*

**Correspondence Author: trunal.bhujangrao@tecnalia.com; Tel.: +34 610 845 819*

Abstract:

The experimental characterization of the material under shear loading is essential for researchers to study the plastic behavior of materials during manufacturing processes. Indeed, regardless of the loading mode, ductile materials mainly deform plastically under shear loading. Thus, for such material behavior analysis, shear tests are very useful. In this paper, a test procedure is defined to characterize the shear deformation of AA7075 aluminum alloy at high strain under compression loading. The Finite Element (FE) simulation is used to select the suitable specimen geometry for the testing. Finally, the experimental tests are carried out using a conventional compression device at a constant strain rate of 0.1 s^{-1} and at an elevated temperature of 20 °C to 500 °C. The results show that the drop in the flow stress curved relative to the increase in temperature exhibits the softening mechanism. The homogeneous behavior of the shear strain along the shear region was also observed and shown by the macro and micro images. The effect of temperature and equivalent strain on the evolution of the microstructure is discussed in detail. It is discovered that, various dynamic recrystallization mechanisms were recorded for aluminum alloy AA7075 depending on the imposed strain conditions.

Keywords: Shear compression test; large deformation; FE-simulation; edge effect; AA7075 alloy; dynamic recrystallization.

Declarations

Funding: This project received funding from the European Union's Marie Skłodowska–Curie Actions (MSCA) Innovative Training Networks (ITN) H2020-MSCA-ITN-2017 under the grant agreement N◦764979.

Conflicts of Interest: The authors declare no conflict of interest.

Availability of data and material (data transparency): Not applicable

Ethics approval (include appropriate approvals or waivers): Not applicable

Consent to participate (include appropriate statements): Not applicable

1. Introduction

The understanding of the material behavior under shear loading has great importance for a researcher in manufacturing processes like cutting, machining, milling, turning, friction stir welding (FSW), etc., where the material experiences large plastic deformation. For such material behavior analysis, hot shear tests provide a useful means to investigate the evolution of the microstructure at a wide range of temperatures and also contribute to improving the material behavior model.

Over the last decades, shear loading properties of materials have been investigated intensively by various testing methods. The most common method is by direct shear loading (e.g., torsion test) and by simple shear test (e.g., using appropriate specimen design to convert a tensile or compressive load into shear). However, the simple shear test has several advantages, it eliminates necking or barreling in the specimen, with no Poisson-ratio effect, and it is easy to achieve high strain and high strain rate in the shear region of the specimen [1] [2].

Many research studies show that various specimen geometries are used to characterize material behavior in shear. The first simple shear specimen was developed by Hundy and Green [3] under tensile loading to convert tensile load into shear. Subsequently, Meyer and Manwaring [4] designed the "Hat specimen" to study the shear localization behavior for compressive loading, and later, this specimen was modified and used by many other researchers. Another group of a specimen such as double shear specimen [5], single or double edge [2], step or dumbbell [6], Compact Forced-Simple-Shear (CFSS) [7], truncated conic [8] and indentation [9] were designed to study the shear behavior of the various metals and alloys. Dodd et al. [10] gave a detailed critical review on different kinds of shear specimens with their advantages and disadvantages. Peirs et al. [11] presented the eccentric notched shear specimen; it was designed for shear testing of sheet metal over a wide range of strain rates. Brosius et al. [12] introduced a specimen geometry called the double-bridge shear specimen. Isakov et al. [13] used a modified specimen geometry based on ASTM B831.

Although most of these shear specimens concern only the material's elastic response, none of them studies the plastic behavior under large deformation. Plastic deformation is much more complex and is more strongly dependent on strain rate, temperature, deformation, etc. It is increasingly important to capture the plastic response of the material in order to develop an accurate model of the material. However, the state of large equivalent strain with a dominant shear strain is not easily achievable in shear specimens.

Rittel et al. designed a unique Shear-Compression Specimen (SCS) for the large strain and a wide range of strain rate [14] [15], the specimen is designed which converts the compression load into the shear load in the gauge section of the specimen. It was reported that the stress (strain) state in the gauge section of SCS is three-dimensional but dominated by the shear during cold deformation. Recently, Moemeni et al. [16] studied the flow behavior of a magnesium alloy with SCS during hot deformation at the quasi-static regime. They pointed out that the shear strain dominated the whole process of the deformation, and large deformation is easily achievable. Nevertheless, they did not discuss the geometrical instability (e.g., edge effect) that occurred during the large plastic deformation [17]. In case of large deformation, as the applied deformation increases, buckling is observed in the gauge section of the specimen due to edge effect, and this geometrical instability can influence the shear strain data in the shear region if the careful design of the specimen is not done. It is therefore important to choose an appropriate specimen dimension for the shear compression test. In this article, the hot behavior of AA7075 alloy is studied by using a new modified specimen geometry, which is based on the specimen geometry given by Rittel et al. [14].

AA7075 alloy is the most widely used alloy in aerospace industries due to its high mechanical strength, lightweight, dimensional stability, machinability, and excellent vibration-damping characteristics. Hence this alloy will be the focus of this research. Many researchers studied the behavior of the AA7075 alloy under different strain rates and at high temperatures

[18, 19, 20, 21, 22]. However, there is not much information available on the microstructure evolution of AA7075 alloy at large deformation under shear loading.

This paper is organized into two different parts. In the first part, a new shear specimen geometry is proposed. It is verified numerically using FE simulation to validate the geometrical aspect of the specimen for large plastic deformation to obtain the homogeneity of the shear strain along the shear region. The new shear specimen is then tested experimentally at elevated temperature, and the experimental results are analyzed. The second part of this paper studies the metallographic microstructure behavior of alloy AA7075 based on the softening mechanism (such as dynamic recrystallization), which takes place during the hot deformation, and to investigates the effect of different strain levels on the evolution of microstructure.

2. Materials and Methods

2.1. Shear specimen geometry

The shear specimen geometry selected for this work is inspired by Rittel et al. [14] for large deformation under shear compression loading. It consists of a planner specimen with a gauge section created by two opposing 45° notches through the specimen thickness. The existing specimen geometry is designed to perform the quasi-static and dynamic test. However, this sample geometry was not well investigated by the researcher with respect to the large deformation at high temperature and the associated geometric instability, such as edge effect and barreling of the specimen.

The schematic representation of the simple compression shear test is shown in Figure 1. Once the compressive load is applied to the upper surface of the specimen, one of its force components is transformed into the dominant shear load in the shear region. The material closed to two opposite corners of the shear region subjected to transverse tension. At the same time, the material close to the other two corners is subjected to compression. Contrarily, around the

corners of the notch, where transverse compression occurs, one can observe an initiation of buckling. The shear strain is constant in the middle section of the shear region as in the free ends of the notch, where it decreases. This phenomenon is called an edge effect. Hence, for large shear deformation, the shear strain data at the mid-section of the shear region are often influenced by this edge effect, if the specimen's design is not carefully done. According to the buckling theory, the critical stress for which buckling occurs is inversely proportional to the buckling width (w) and linearly proportional to the length (L). Therefore, it is important to select the appropriate dimension of the shear region such as length, width, thickness, height, shape, and size of the specimen to avoid edge effect or buckling to achieve homogeneous shear strain in the shear region for large plastic deformation.

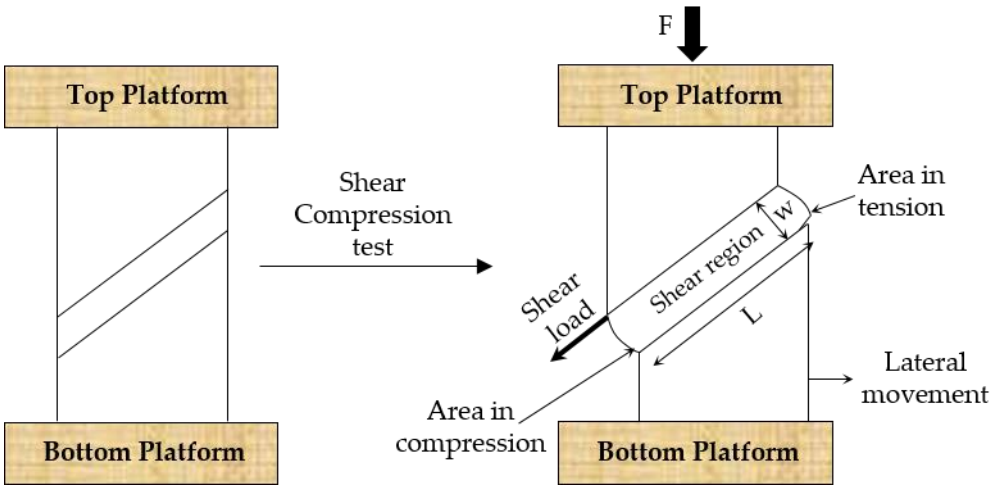

Figure 1:The schematic representation of a simple shear compression test.

Furthermore, as shown in Figure 1, the specimen is placed between the flat compressive platforms. When the load is applied to the top platform, the compressive load converts into a shear load in the notch section; at the same time, one of its load components allows the specimen to move in the lateral direction. From Figure 1, it can be seen that the specimen slightly moved in a lateral direction. However, this movement is limited by the friction between the specimen surface and the flat compression platform. If a specimen does not move in the lateral direction,

premature failure may occur by cracking along the notch or undergoing pure compressive deformation instead of in shear. Therefore, it is of interest to study the effect of surface contact between the specimen and flat platform on the shear strain of the specimen.

2.2. Finite element simulation

The starting point for the design of the new shear specimen is to select the appropriate geometrical parameters of the shear region or notch section. The numerical FE-simulation was performed for various geometries of the specimen by considering different values of length (L) and width (w) using ABAQUS software. The results are obtained to demonstrate the effect of equally distributed plastic shear strain (PE12= Plastic strain in 12 direction or shear direction) in the mid-section of the shear region during the entire loading history. The most representative developed simulations are presented in this paper. The specimen is meshed using the 3D solid element of C3D8R type. It is the 8-node linear brick element with reduced integration and hourglass control. The mesh at the gauge section is kept dense with a seed size of 0.2 mm. The longitudinal compressive displacement of 5 mm is applied to the upper face of the specimen.

The specimen places on the flat rigid compressive platform. The surface friction (μ = 0.3 [23]) contact property is given to the surface of the specimen and flat platform surface, and the platform is fixed in all directions. The vertical loading displacement of 5mm is applied on the upper surface of the specimen. The simulation time is fixed to 10 sec, like in the quasi-static test. The material constitutes response was model by using the elastic-plastic material model. The most common material models used in the literature are based on the plasticity approach, e.g., Power-law [24], Zerilli-Armstrong [25], Steinberg and Guinan [26] etc. However, no single material model represents a large variety of materials that undergo large deformation, different strain rates, and elevated temperature for the simulation. In contrast, the Johnson-Cook

(J-C) model is the most widely used material model for simulation in the industries. It has more practical applications, mainly due to its simple form; easy to calibrate and implement.

$$\sigma = (A + B\varepsilon^{n}) \left(1 + C \ln(\frac{\dot{\varepsilon}}{\dot{\varepsilon}_0})\right) \left(1 - \left(\frac{T - T_0}{T_m - T_0}\right)^{m}\right) \quad (1)$$

In this work, the effect of stress and temperature on the hardening behavior of the material is described by the J-C model. The material properties of the AA7075 alloy are listed in Table 1. The temperature rise is taken into account in the simulation. The deformation heating by plastic work is included in the given model of the loaded specimens. The quasi-isotropic and adiabatic temperature increase in the specimen during high to low strain rate plastic deformation is calculated using the following formula:

$$\Delta T = \frac{\beta}{\rho C} \int \sigma d\varepsilon_p \quad (2)$$

In this equation, ρ is the mass density, c the specific heat and β the Taylor-Quinney coefficient indicating the fraction of plastic work converted into heat. This β value is usually assumed to have a value between 0.9 and 1 , here 0.9 is used.

Table 1:Material properties of AA7075 [27, 28]

Youngs Modulus (MPa)	70000
Poisson´s Ratio	0.3
Melting Temp (°C)	520-635
Density (tonne/mm3)	2.70E-09
Heat Capacity J/K/kg	960
Heat Conductivity, λ (W/m/K)	130
Taylor Quinney coefficient (β)	0.9

Brar et al. [29] and Zhang [30] evaluated the J-C parameters for the AA7075 alloy based on the Equation 1 by performing the quasi-static and split Hopkinson pressure bar tests at various strain rates and temperatures. For the present study, the J--C parameter values such as A, B, C, n, m are taken from the work carried out by Zhang [30], listed in Table 2.

Table 2:Johnson-Cook parameters for AA7075 alloy [30]

A (MPa)	B (MPa)	n	C	m
473	210	0.3813	0.033	1.56

2.3. Specimen Optimization

The results obtained from the numerical simulation on the different geometries of the shear compression specimen are discussed in this section. The first observation shows that, as a result of the vertical compressive loading, there is local vertical displacement in the shear region [14]. In addition, the American Society for Testing and Materials (ASTM) and the International Organization for Standardization (ISO) have different standards for cylindrical and rectangular compression specimens. In this article, the standards chose based on ASTM E209-18, commonly used for compression testing of metallic materials at elevated temperatures with conventional or rapid heating and deformation rates. Specimens of any thickness (in this paper, it is notch thickness) up to 14 mm but not so thin and the length to breadth ratio (L/b) of the specimen should be approximately 1.4. However, from the literature is found out that there is no specific standard for high temperature shear and compression test specimens. Once the load increases, the material in the notch section begins to flow in the shear direction rather than vertically. Hence, this limited displacement is minimal; there is no effect on the shear deformation of the specimen due to initial displacement. The influence of some geometrical parameters of the specimen on the shear strain behavior is given below.

Influence of the length of the notch:

FE-simulations were performed on different lengths (L) of the notch section, from 30 mm to 100 mm with a constant width (w) of 5 mm. Figure 2 shows that the plastic shear strain (PE12) is quite homogenous in the central part of the notch section for both specimens, except at the end of the notch, where the shear strain reduced. The black circle shows the edge effect

at the end of the notch. However, the plastic shear strain in the large L specimen is much lower than in the small L specimen. It is also observed that the width of the shear zone for large L specimen is considerably reduced under the same loading conditions. This means the large L specimen possibly undergoes more deformation in the vertical direction (PE22= Plastic strain in vertical direction or in this case compression strain) than in the shear direction (PE12) and does not allow the material to flow in the notch section.

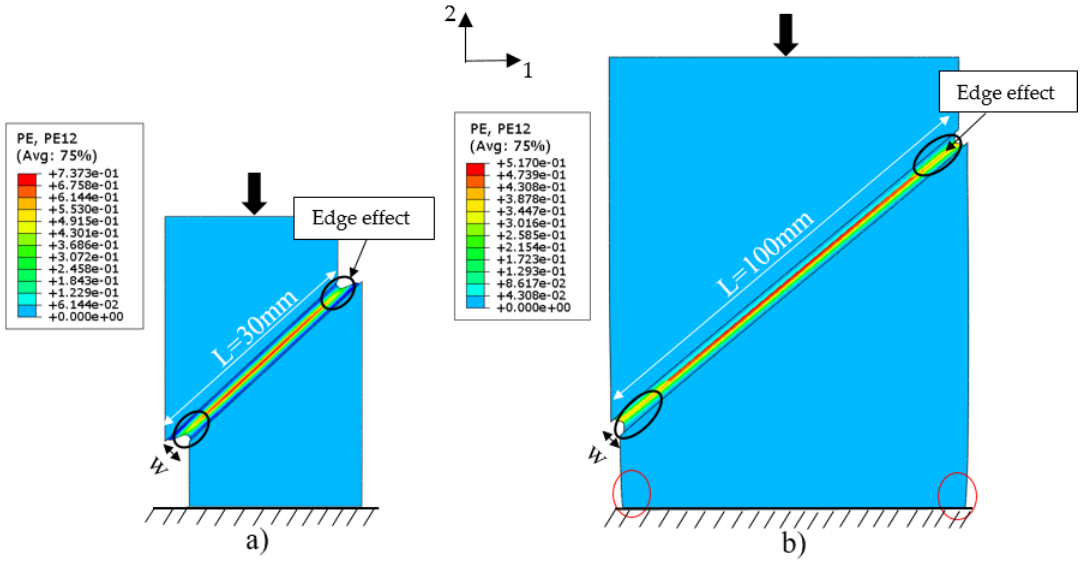

Figure 2:Simulation results of different lengths of the notch with the constant width = 5mm, a) small specimen with length of 30mm and b) large specimen with the length of 100mm

Furthermore, the mesh near the lower corners of the large L specimen appears to be coarsened, as shown in Figure 2 (red circle). It is assumed that friction between the specimen and the flat platform limits the lateral movement of the specimen and allows the specimen to bend at the corner. Compared to the small L specimen, the large L specimen undergoes more bending due to large surface contact. This restriction of movement may create compression in the notch section; hence, it is necessary to carefully design the test conditions.

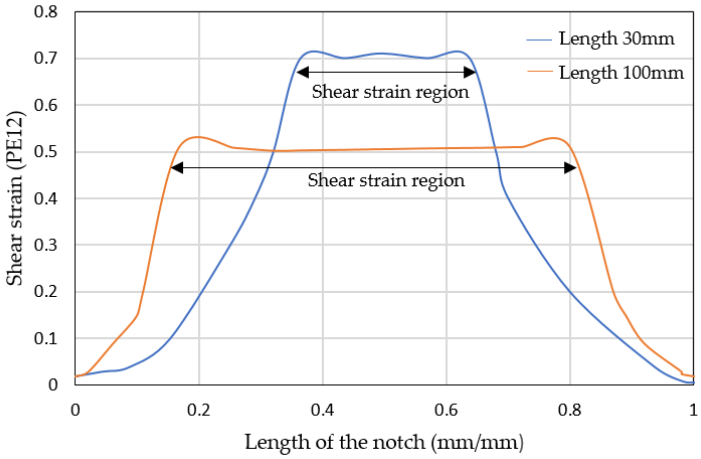

Figure 3:The homogeneity of the shear strain along the length of the notch

From figure 3, it can be seen that if the length of the notch section is reduced, the region where the constant shear strain can be observed begins to decrease. Therefore, it is necessary to have a sufficient length of the notch to observe the shear deformation in the notch section. Besides, the level of shear strain is controlled by adjustment of the total height reduction of the specimen.

Influence of the width of the notch:

A similar FE-simulation is performed on different widths (w) of the notch, such as 5 mm and 7 mm with constant length (L = 30 mm). As shown in Figure 4, the plastic shear strain (PE12) is visually identical in the mid-section of both specimens without the dominance of compressive strain. It means that the plastic shear strain is independent of the notch width. The edge effect is clearly shown in both specimens, whereas a shear strain is maximum in the central part of the notch region compare to its end. However, the width of the notch should not be very large comparing to the length of the specimen, and it may undergo compression instead of shear.

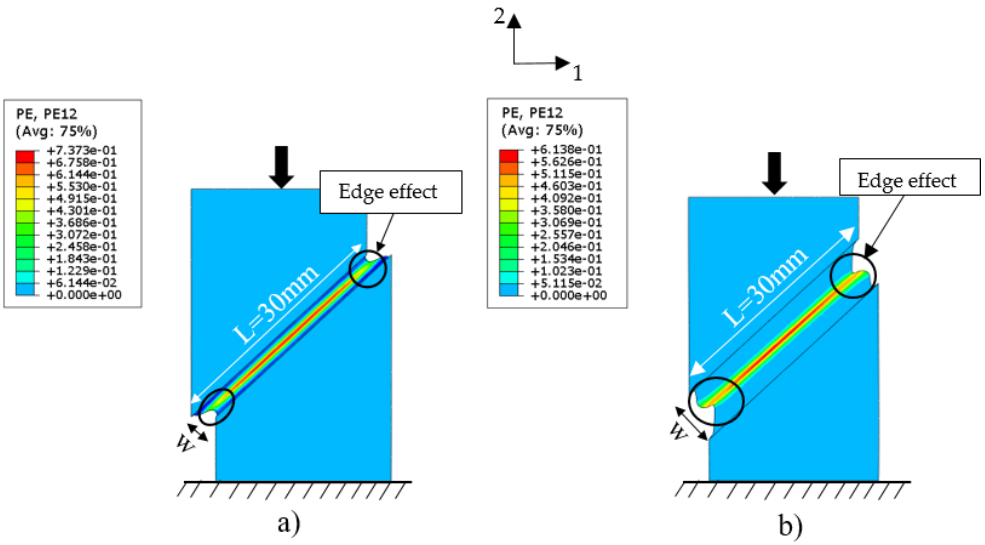

Figure 4:Simulation results of different widths of the notch with similar length=30mm: a) Specimen with width of 5mm b) Specimen with width of 7 mm.

By summarizing the selection of length (L) and width (w) of the notch, the following conclusions are drawn:

1. In order to achieve accurate shear strain data along the notch section, the length of the notch should be neither very large nor very small. For large L specimen, the more area is available to observe the shear strain. However, the level of shear strain is lower due to local compression that occurred in the notch section and maybe due to the barreling effect at the bottom corner. In addition, the specimen size required for the large L is quite big, while for the small L specimen, the observation area of the shear strain is very short.
2. During the shear compression loading, the careful design of the flat compressive platform must be done to obtain frictionless lateral movement of the specimen. This can be achieved by using lubricant at a high temperature [31, 32], which allows the specimen to move freely during loading.
3. For the width of the notch, the width should be large enough in order to have a sufficiently representative sample of the material subjected to shear. A larger width also simplifies the use of optical methods to measure the strain. However, if the width of the notch is very large in relation to the length (L), the shear strain data can be influenced by the edge effect.

To illustrate the extent of effect of L/w ratio, finite element simulation of simple shear test were carried out for various geometries as explained before, namely for different values of L/w. e.g. some simulations are presented in figures here Figure 5.(S12=Stress component in 12 direction also called shear stress, PE12= plastic strain component in 12 direction also called as plastic shear strain)

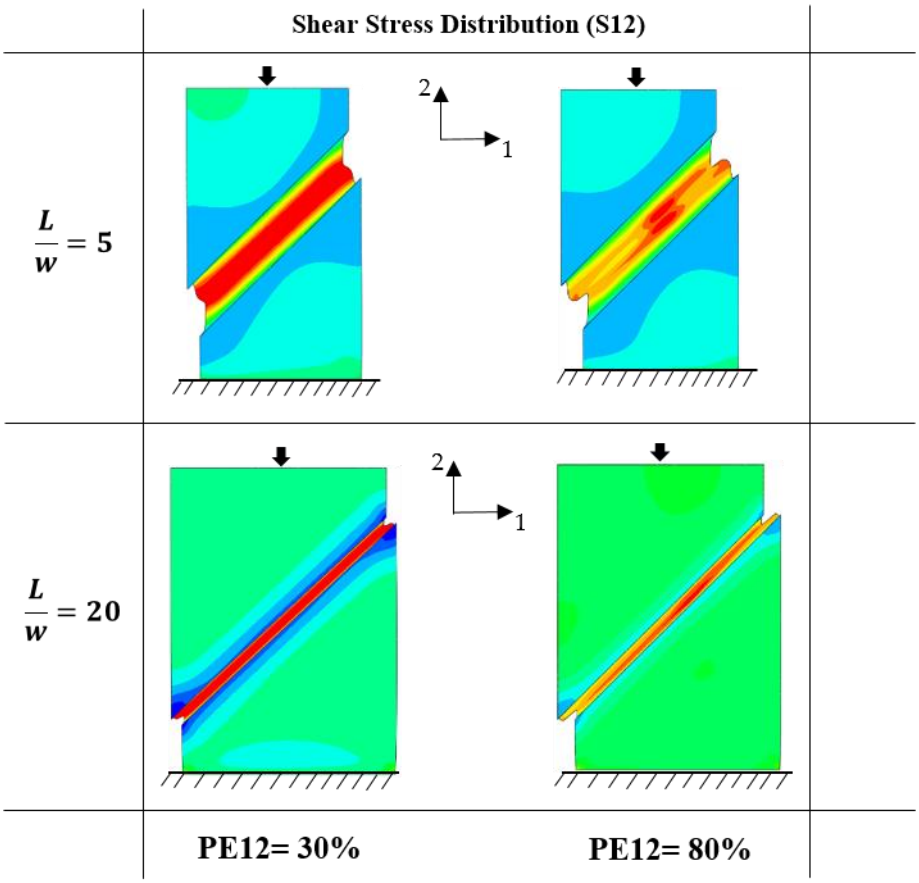

Figure 5:Distribution of the shear stress S12 (MPa) in a shear test, after different amounts of shear strain (PE12) and different geometries of the sample based on L/w ratio.

The main conclusions that can be drawn from the above results are:

- The shear stress distribution is quite homogeneous in a large part of the specimen. The shear strain is rather constant over the gauge area, except near the free ends, where it decreases.

- The shear stress distributions S12, Figure 5 show that reducing the notch area width produces a decrease in the influence of the free ends, while enlarging the notch area length increases the size of the regions of homogeneous behaviour.
- The heterogeneity of the shear stress/strain increases with the amount of shear whatever the value of the ratio L/w. However, the size of the heterogeneous areas increases with the decrease of the L/w ratio.

The finite element simulations have shown that the simplest way to reduce the stress and strain heterogeneity is to modify the geometry of the specimen. Indeed, on the basis of the calculations carried out, and it is assumed that in order to minimize the influence of the free ends (edge effect) and to induce an almost homogeneous state of stress in the notch part, the length-over-width ratio L/w has to be greater than and equal to 10 for metallic materials. Indeed , L/w ratio must be chosen by respecting the standards of the compression test e.g based on the clamps, load cell of the testing machine, etc. Therefore, by performing FE-simulations on various geometries of the specimen, and considering the above criteria, the optimal length and width of the notch is determined and is given in Section 2.4.

2.4. The final design of the specimen

The final design of the specimen is shown in Figure 6; it consists of a flat rectangular bar shape with a total height (H) of 60 mm and a cross-section of 30 x 15 (b x k) mm specimen. The double notch was machined at 45° with a circular shape of radius r = 2 mm on opposite sides. The width of the notch section is considered as $w = 2r = 4$ mm. The vertical height of the notch is $h = 2\sqrt{2}r = 5.65$ mm. The length of the notch is L = 42.43 mm, which gives the length over width ratio of $L/w \geq 10$, [16] also recommended a length over width ratio L/w of at least 10 in order to have homogenous shear strain distribution along the shear region.

The thickness (t) of the notch cannot be arbitrarily small, and the thickness must be a multiple of the intrinsic scale of the material, such as grain size in metals [33]. For a greater thickness, a higher load is required to deform the specimen. Thus, the recommended thickness is considered to be t = 5 mm. It is large enough to measure the amount of load per given load cell at high temperature and can be deformed without early fracture and ensures that the material in the shear region deforms plastically in the shear direction. The length of the specimen subjected to the test load is 42.43 mm.

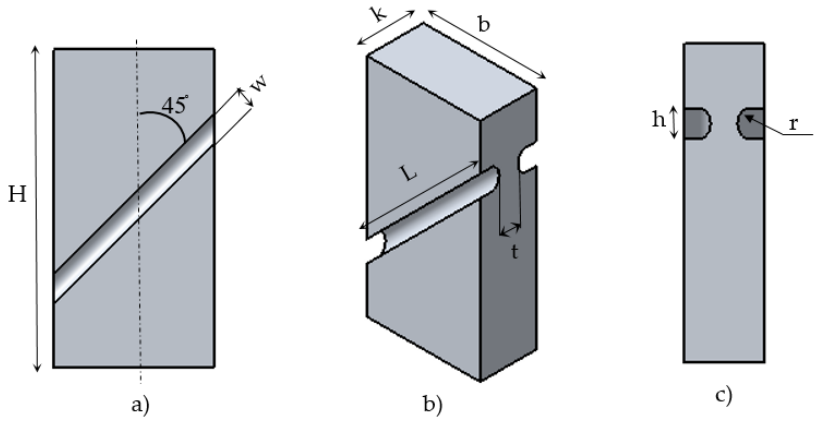

Figure 6:Shear compression specimen with a) front view b) isometric view c) side view

The position of the notches against the axis of symmetry has a significant effect on the stress state in the shear region. The idea here is to convert longitudinal compression of the specimen into the dominant state of shear load in the gauge section. Hence, notches are created at the angle of 45° on the opposite side of the specimen, and it allows the material to flow inside the notch section. Thus, care must be taken when manufacturing the position of the notch.

The shape of the notch is also very important in order to avoid any early fracture and transfer only shear load. It was found that the radius of the notch depends entirely on the width of the notch (w=2r) as it is directly proportional. If the width increases, the radius will increase. The effect of the notch radius was therefore not studied separately, instead the effect of the width is examined in this paper.

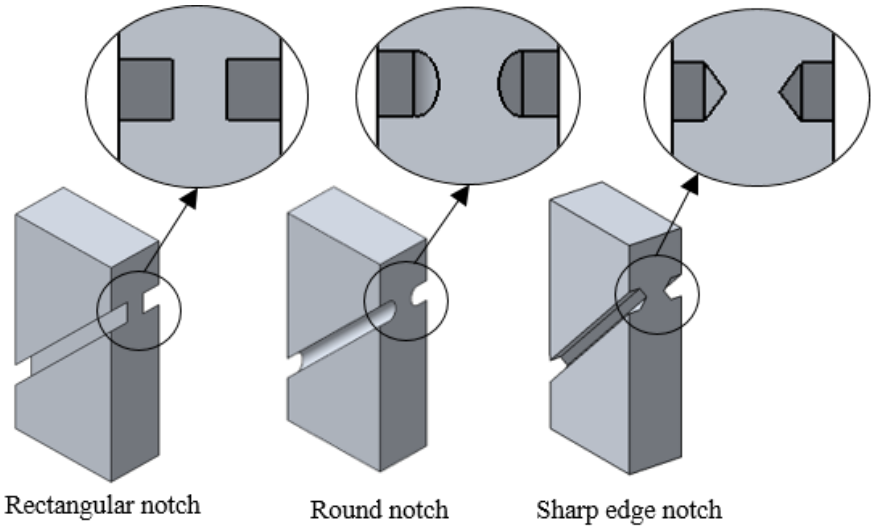

Figure 7:Different geometries of notchs

However, the effect of the shape of the notch has significant effect on the shear stress and strain. Based on the specimen geometries found in the literature [18, 34],The most common used shapes of the notch are rectangular, round and sharp edge shape shown in Figure 7. However, the notch with rectangular and sharp edge shape have some limitations; it consists of stress concentration areas (edge part). Therefore, failure and fracture are always forced to occur in those regions. Whereas in the round shape type, the stress concentration is minimized and secured from early facture., Also, the strain is constant throughout the shear region for a larger shear strain. Hence the circular notch shape is used in this work.

2.5. Evaluation of equivalent stress and strain in the shear region

After the design of the new shear specimen, a final FE-simulation was performed to demonstrate the shear stress and strain components referred to the center of the notch section for AA7075 alloy. The notch has a width of 4 mm and a length of 42.43 mm. The 5 mm of vertical displacement is applied numerically on the top surface of the specimen. A hard contact behavior and a frictionless interaction property are used between the flat bottom platform and the specimen surface in order to allow the specimen to move freely in the lateral direction during loading.

The stress and strain fields are of three-dimensional nature, which cannot give a simple analytical description of simple shear. Hence, the equivalent stress (von Mises) and the equivalent plastic strain (PEEQ) are determined for the representation of the stress and strain. The equivalent plastic strain is the ratio between the applied displacement (Δd) of the specimen and width (w) of the shear region. Figure 8 confirms the relative uniformity of the equivalent stress and strain fields in the gauge section without any geometric defect (e.g., bending at the bottom) in the specimen. However, a slight edge effect was observed at the end of the notch, where shear strain is decreased. This does not influence the shear stress-strain data of the notch region, and the shear component is more dominant in the mid-section of the notch region, which is PE12 = 1.02, and there is no bending occurred at the bottom of the specimen.

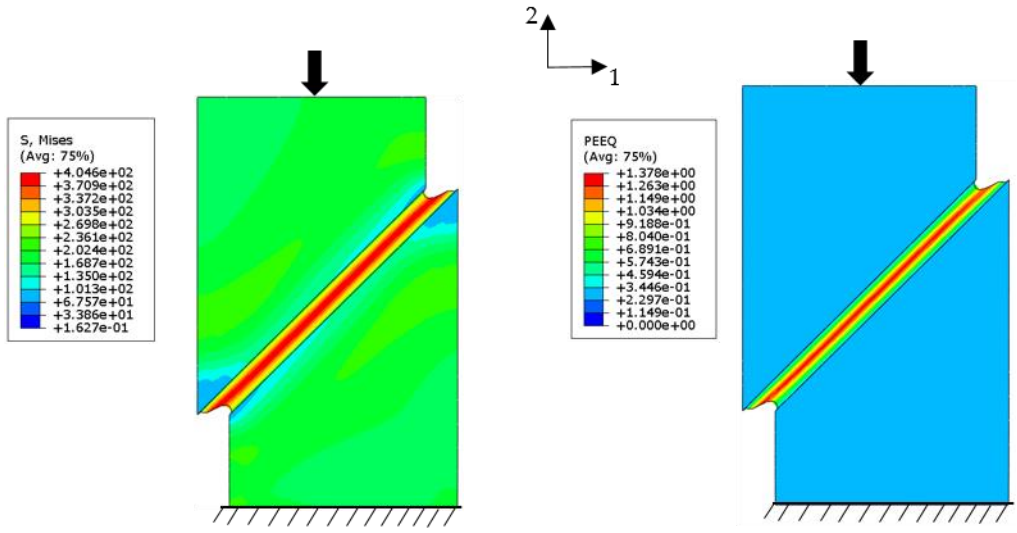

Figure 8:Homogenous von Mises equivalent stress (on the left side) and plastic shear strain (PEEQ) (on the right side) shown in the notch section

2.6. Experimental Setup

For the quasi-static shear compression test, the conventional compression setup is used. The specimens are extracted from the as-received AA7075 alloy rectangular plate with a thickness of 15 mm and cut into smaller samples using an electric discharge machining (EDM). The chemical compositions of AA7075 alloy used in this work are given in Table 3 [28].

Table 3:Chemical composition of AA7075 in weight % [28]

Element	Zn	Mg	Cu	Cr	Fe	Mn	Si	Ti	Al
Wt. %	5.6-6.1	2.1-2.5	1.2-1.6	0.18-0.28	Max 0.5	Max 0.3	Max.0.4	Max.0.2	bal

The hot shear compression test is carried out in order to impose higher shear deformation using the Instron testing machine equipped with a load cell of 100 kN. The heating device is mounted on the testing machine to perform the test at a high temperature (the heating device range is up to 600 °C), as shown in Figure 9.

A crosshead speed of 33.6 mm/min was used for all tests, which correspond to a strain rate of 0.1 s^{-1}. The tests were conducted at temperatures of 25 °C (room temperature), 300 °C, 400 °C, and 500 °C. The specimens were heated at a rate of 5 °C/s to the desired deformation temperature and were held for 300 seconds at that temperature to achieve homogeneous temperature distribution throughout the sample. The temperature is accurately controlled by a K-type thermocouple attached to the surface of the specimen. The shear strain level and the equivalent strain were controlled by adjusting the specimen's vertical height reduction.

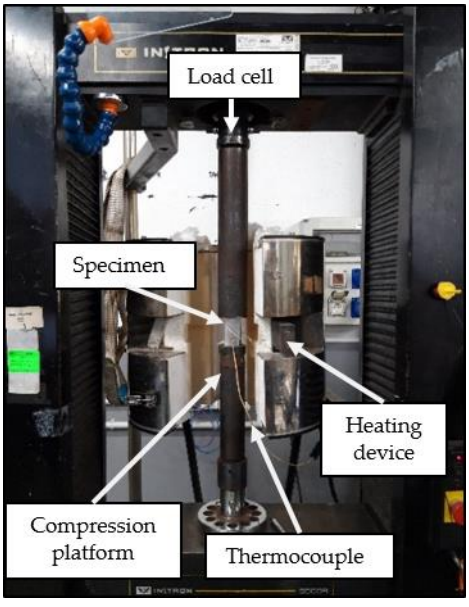

Figure 9:Experimental setup and heating device

In order to eliminate the lateral friction between the specimen surface and the surface of the platform, the high-temperature resistance lubrication gel is used on both surfaces, which

allows the lateral motion frictionless (μ = 0.06). The interrupted test was also performed at 500 °C to study the evolution of the microstructure of the material at a different strain level.

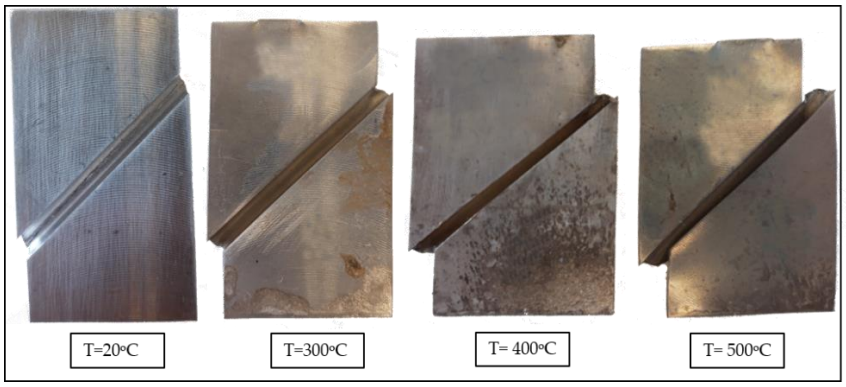

Figure 10: The deformed specimens at the different temperature

The deformed specimen at different temperature shown in Figure 10, At 20ºC, the specimen fracture very early and the crack is propagated from the edge of the notch. As the temperature increases, the more deformation was imposed on the specimen and also the edge effect is clearly seen at the edge of the notch.

The hot deformed specimens were water quenched as soon as the specified amount of strain was imparted (within a few seconds) in order to freeze the hot deformed microstructure. The specimens were mechanically cut along the longitudinal direction using a precision cutting machine to prepare samples for microstructural analysis. The cut surface was mechanically polished for optical metallographic examination and etched using Barker's reagent; it is a diluted fluoroboric acid solution. This electrolytic etching for aluminum alloys allows the observation of the grain size, the undeformed and deformed part of the specimen.

3. Results and discussions

3.1. Flow stress behavior

The force and displacement data can be easily available from the experimental test. The stress-strain plots for the entire test were generated through computer software. The

compressive force required for the shear specimen is determined by both the specimen material and specimen geometry. However, the most important feature of the specimen is that the position of the notches (45° to the compressive loading) leads to an almost pure-shear stress state up to large strains [16]. It means that the local stress in the shear zone is directly related to the measured test load. Hence, the relation between the applied force and local stress in the shear region is defined directly, except the stress near the end of the notch, whereas the relationship between the local shear strain and displacement is not straightforward. Rittel et al [14] proposed a simple equation to relate the equivalent stress and equivalent plastic strain with respect to the applied force and displacements for shear compression specimen. It is suggested that the equivalent strain is the ratio between the applied vertical displacement (Δd) on the specimen and the notch height (h), whereas equivalent stress is the ratio between the applied compressive force (F) to the area of notch region under loading. The simplified relations between displacement, load, geometrical parameters, and equivalent strain (ε_{eq}) and stress (σ_{eq}) were devised as follows:

$$\varepsilon_{eq} = \frac{\Delta d}{h} \quad , \quad \dot{\varepsilon}_{eq} = \frac{\Delta \dot{d}}{h} \tag{3}$$

$$\sigma_{eq} = k_1 \frac{F}{bt} \tag{4}$$

Where,

Δd= applied vertical displacement,

h = notch height (Figure 6),

F = applied compressive load,

b = specimen cross-section breadth (Figure 6),

t = notch thickness (Figure 6), and

k_1 = constant (0.866 also given in Rittel et al.[10,11])

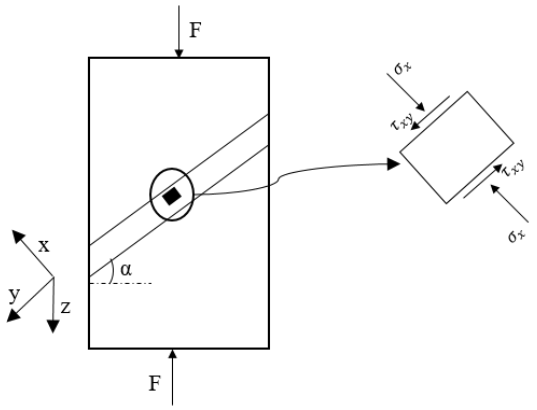

Figure 11:Shear compression geometry and the state of stress at a point within the notch section..

The state of stress within the notch section of shear compression geometry under uniaxial compression (F) for the rectangular sections can be approximated in different ways as shown in Figure 11, here it can be assumed that the continuity of material at the boundaries of the notch section gives rise to a state of uniaxial strain, i.e., $\varepsilon_y = \varepsilon_z = 0$, at least in regions close to notch boundaries. For this case, the stress tensors are given as follows:

$$\sigma_{ij} = \frac{\sigma_{kk}}{3}\delta_{ij} + S_{ij} = \begin{pmatrix} \sigma_x & \tau_{xy} & 0 \\ \tau_{xy} & \frac{\vartheta}{1-\vartheta}\sigma_x & 0 \\ 0 & 0 & \frac{\vartheta}{1-\vartheta}\sigma_x \end{pmatrix} \quad (5)$$

Where,

$$\sigma_x = \frac{F}{bt}cos^2\,\alpha$$

$$\tau_{xy} = \frac{F}{bt}\cos\alpha\, sin\alpha$$

S_{ij} represents the "state of shear", i.e. the state of stress subtracting the hydrostatic pressure part and the deviatoric stress tensor

$$S_{ij} = \frac{F}{bt}\begin{pmatrix} \frac{2(1-2\vartheta)}{3(1-\vartheta)}cos^2\,\alpha & \cos\alpha\, sin\alpha & 0 \\ \cos\alpha\, sin\alpha & \frac{2\vartheta-1}{3(1-\vartheta)}cos^2\,\alpha & 0 \\ 0 & 0 & \frac{2\vartheta-1}{3(1-\vartheta)}cos^2\,\alpha \end{pmatrix} \quad (6)$$

and the equivalent von Mises stress becomes

$$\sigma_{eq} = \sqrt{\frac{3}{2} S_{ij} S_{ij}} = \sqrt{\frac{(1-2\vartheta)^2}{(1-\vartheta)^2} cos^4 \alpha + 3\, cos^2 \alpha\, sin^2 \alpha}\ \frac{F}{bt} \quad (7)$$

Which, for α= 45° and ϑ =1/2 , yields

$$\sigma_{eq} = 0.866 \frac{F}{bt} \quad (8)$$

The comparison of Equation 8 with Equation 4 suggests that k1 = 0.866 in Equation 4. It should be noted that the stress state in this last case Equation 6 reduces to a state of pure shear superimposed by a hydrostatic stress component for ϑ = 1/2, as in the pressure-shear experiments of Clifton and Klopp [35].

The results obtained from the hot shear compression test were analyzed and discussed in detail. The experimental flow stress-strain curve for each test was drawn. The equivalent stress vs. strain graph at a different temperature from 20 °C (Room temperature) to 500 °C shown in Figure 12. It can be observed from the graph that, as the temperature increases, the strength of the material decreases. It is clear that the flow stress behavior is greatly influenced by the temperature, especially at room temperature and below 300°C. The strain hardening behavior was observed at room temperature and continuously decreases after yielding, whereas a sudden drop in flow stress followed by a steady-state was observed in the specimens tested at 300 °C and above. The reason for this is that the effect of strain hardening is more obvious at a lower temperature [36].

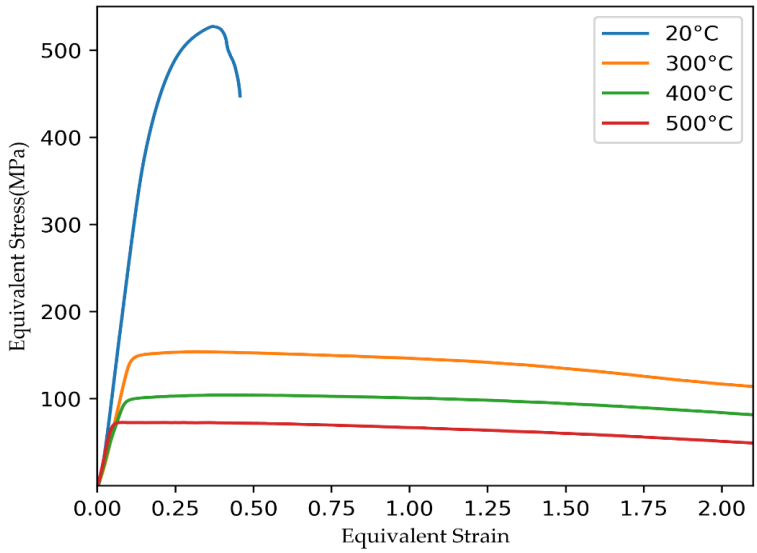

Figure 12:Equivalent stress vs. strain curves for the hot shear compression test at different temperatures with a strain rate of 0.1 s^{-1}.

However, the ductility increases with increasing deformation temperature from 300°C to 500°C. Besides, at higher temperatures, it assumed that the age-hardening precipitates might dissolved in the Al matrix. The absence of the precipitates offers unrestricted motion to the dislocations resulting in the decrease in the flow strength of the material at higher temperatures. The material appears to have undergone a softening mechanism during the deformation process characterized by a decrease in flow stress after deformation of about 0.2 and after it has reached a stable state. This means that the flow stress behavior is significantly influenced by the softening mechanism.

The softening mechanism observed in the AA7075 alloys are especially due to Dynamic Recovery (DRV) and by Dynamic Recrystallization (DRX) [37, 38]. The DRV occurs at the initial stage of softening, and DRX acts predominantly at a higher temperature. Several mechanisms of dynamic recrystallization have been reported for aluminum alloys depending on the imposed deformation conditions [10, 12, 13]. The recrystallization process was considered as the main mechanism of microstructural evolution [16, 17].

The materials with high stacking fault energy (SFE) such as AA7075 alloy normally undergoes Continuous Dynamic Recrystallization (CDRX) where the subgrains with Low

Angle Grain Boundaries (LAGBs) are formed during deformation of the material, which progressively transforms into grains with High Angle Grain Boundaries (HAGBs) as the deformation increases. There exists another type of DRX named Geometric Dynamic Recrystallization (GDRX), which is observed, for instance, on deforming aluminum alloy to very large strains at elevated temperatures. In this case, the deformed grains become elongated with local serrations, and as the deformation increases, equiaxed grains are formed by the pinching off of serrations [39]. Therefore, a set of experiments was carried out at 500°C with different equivalent strain levels (0.6, 1.2, 2.1) followed by the microstructure characterization to observe the evolution of DRX and the effect of deformation temperature on the softening mechanism is discussed in the next section.

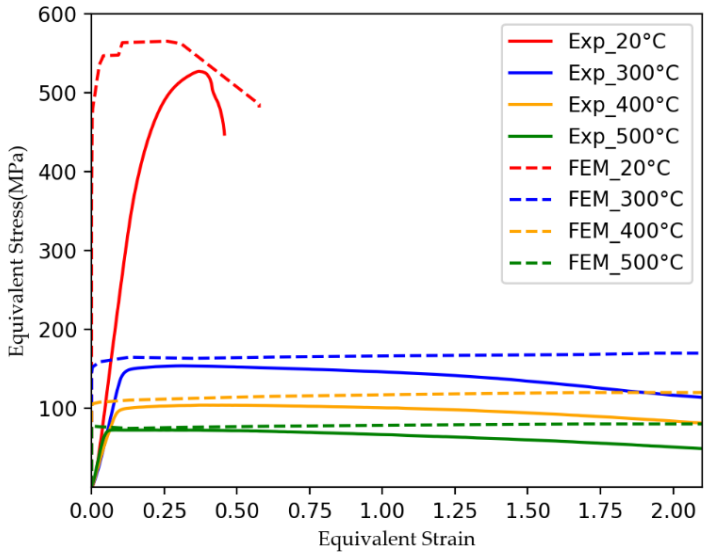

Figure 13:Equivalent stress-strain curves obtained from experimental and numerical simulation at different temperatures with a strain rate of 0.1 s-1.

The inverse approach to verify the stress-strain curve obtained from the experimental tests and the FEM Model shown in Figure 13. As it can be seen that, there is a satisfactory agreement between the numerical and experimental results except that as the deformation increases the numerical results does not follow the experimental stress strain curve. Which means that for large plastic deformation the assumed constitute law needs to be modified to obtained accurate results. This aspect will be investigated in the recent future.

3.2 Microstructure characterization

3.2.1. Initial Microstructure

The initial microstructure of alloy AA7075 observed in the longitudinal direction (parallel to the elongated grain) of the extruded base plate using an Optical Microscope (OM) is shown in Figure 14. The white intermetallic particles are also found along the grain boundaries.

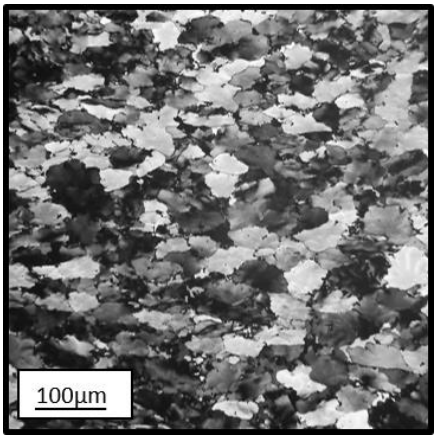

Figure 14:Initial microstructure of AA7075 alloy

The composition of the AA7075 alloy is determined by using EDS (Energy Dispersive X-ray Spectroscopy). Figure 15 (a) shows the typical microstructure of the as-received AA7075 plate sample viewed by using BES (Backscattered Electron Scanning). The zoomed black color dotted square area depicted three types of constituent particles: coarse white particles (inside a red color circle), black particles (inside the yellow color rectangle), and Al matrix (inside the green square) as shown in Figure 15 (b). These particles do not seem to have any particular shapes and appear to be present along the grain boundaries.

EDS scans were performed over an area (EDS Map) and at a point (EDS Spot) to obtain the nominal chemical composition of the Al matrix and the white intermetallic observed in the grain boundary, respectively, which are listed in Table 4. This is only a semi-quantitative presentation without more standardization. So, ~ ±3 to ±6 % variation in Al, Zn, Mg, and Cu contents found in this study are consistent with that of general AA7075 reported in Table 3.

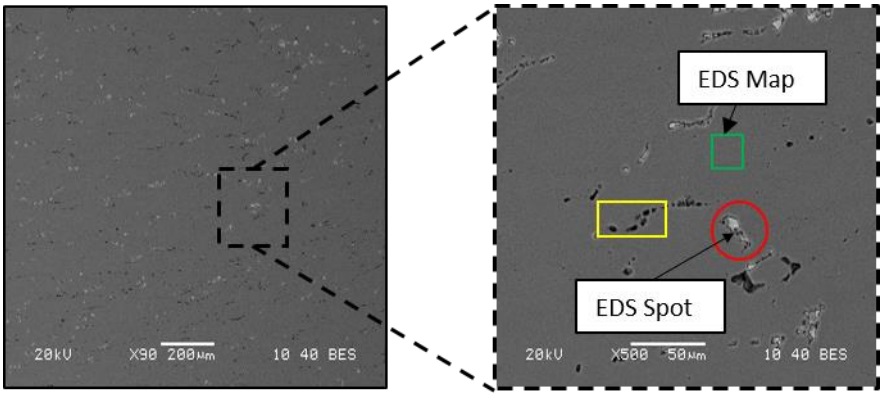

Figure 15:(a) BES image of the AA7075 sample, and (b) Magnified BES image depicting the coarse bright and dark intermetallic in the microstructure

Table 4 shows that the white intermetallic in the Al-matrix mainly consists of Al, Fe, Cu, and Zn. Their weight % suggested that the empirical formulae of the intermetallic might be Al28CuFe3. T.M. Yue et al. [40] also reported identical second phase particle Al23CuFe4 in AA7075 material. These Fe-rich phases are formed in the alloys that contain Fe as an impurity. However, the second type of intermetallic contains Si and Mg as primary elements along with a small amount of O and Al and appears darker than the Al matrix. A typical example of this type of inclusions is Mg2Si [41]. These intermetallic particles can be formed during the manufacturing process. They play an important role in the strength of the material. In addition, as the deformation temperature increases, the solubility of the alloy elements in the matrix increases, a large number of particles dissolved in the matrix, which was beneficial for the grain boundaries to slide or move [39] and enables the large plastic deformation. More EDS maps still need to be captured to analyze the composition of the other second phase particles and the precipitations such as the η phase (MgZn2), η´phase (MgZn), etc. and systematic studies are required to understand the effect of these phases on microstructure evolution.

Table 4:Chemical composition of Al-matrix and white intermetallic

Elements	Al-matrix [EDS Map]			White particles [EDS Spot]		
	Mass %	Atomic %	Error %	Mass %	Atomic %	Error %
Al	90.65	93.87	4.8	71.67	84.05	4.8
Zn	4.74	2.02	3.36	2.51	1.21	3.94
Mg	2.76	3.18	6.4	0.66	0.85	9.55
Cu	1.38	0.61	4.84	6	2.99	3.17
Fe	0.18	0.09	17.97	17.71	10.03	2.8
Si	0.16	0.16	20.44	0.04	0.05	8.1
Mn	0.13	0.07	22.81	1.41	0.81	4.59

3.2.2. Effect of temperature and equivalent strain on microstructure

A material becomes thermodynamically unstable during the deformation process due to the increase in the number of defects such as dislocations and interfaces, which increases the energy stored in the system [22]. When it is deformed at elevated temperatures, the free energy of the system is reduced by the removal of these defects through thermally activated processes. The microstructure and the properties of the material can be partially restored to their original values by recovery through annihilation and rearrangement of dislocations. Recovery processes may take place during deformation, which is known as dynamic recovery (DRV) [42]. The deformation heating is also taken into account in the given experimental tests. The increase in temperature at the surface of the specimen during plastic deformation was analyzed using a thermocouple. However, in this paper, the experimental tests are carried out at a very low strain rate of 0.1 s^{-1} (isotropic heating during the deformation) and the rate of temperature increase was found to be much lower than that of 15˚C at different temperatures. Therefore, the it is assumed that thermal softening (the dynamic recrystallization) is mainly due to the given external temperature and partly achieved by the self-rise temperature during plastic deformation.

Figure 16 shows the effect of temperatures on the microstructures of AA7075 alloy at a strain of 2.1 and a strain rate of 0.1 s^{-1}. The microstructure images are taken from the mid-section of the notch in the longitudinal direction of the shear loading. It shows that the grains

are excessively elongated at elevated temperatures in the direction of shear loading, exhibiting large plastic deformation. At a lower temperature such as 300 °C, recrystallization mainly occurred in the grain boundaries, and dynamic recovery is the main mechanism to annihilate dislocations. With the increase in temperature, the generation of new grains was more obvious. At 400 °C, it shows that the recrystallized grains in the grain boundary are increased, and it increased again with increasing temperature, indicating that recrystallization is prone to occur more at a higher temperature.

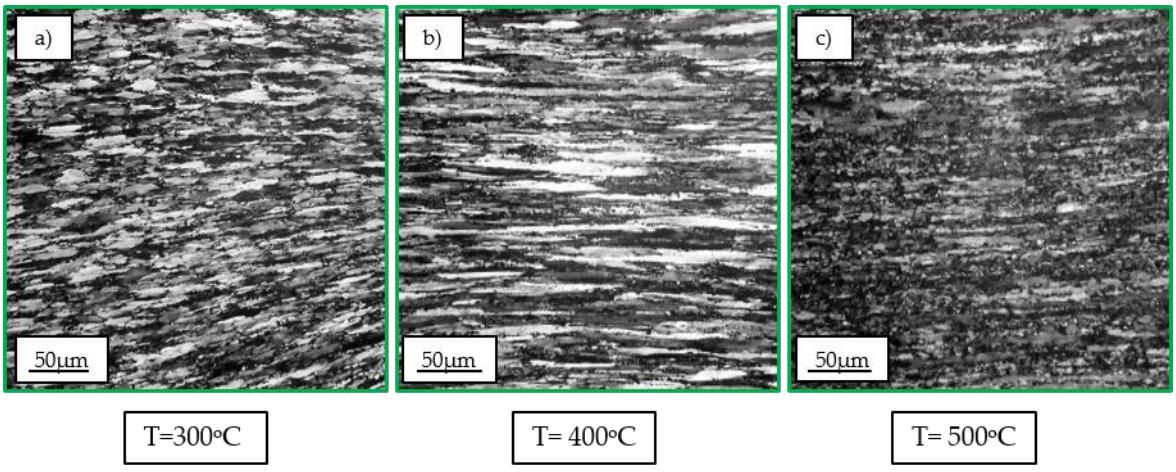

Figure 16:Microstructures of AA7075 alloy at different temperatures (equivalent strain of 2.1 and strain rate 0.1s−1): (a) 300 °C; (b) 400 °C; (c) 500 °C.

Figure 17 shows the effect of equivalent strains on the microstructures of AA7075 alloy at a temperature 500 °C and a strain rate of 0.1 s^{-1}. When the equivalent strain was 0.6, see Figure 17 (a), a few subgrains are formed along the serrated grain boundaries and exhibit necklace feature in the interior of the deformed grains. The necklace microstructure is induced by the rapid development of strain gradients near grain boundaries, i.e., the refined grains result from the sub-gains near to the grain boundaries. It is indeed the mechanism of Discontinuous Dynamic Recrystallization (DDRX) [43]; it has the necklace feature.

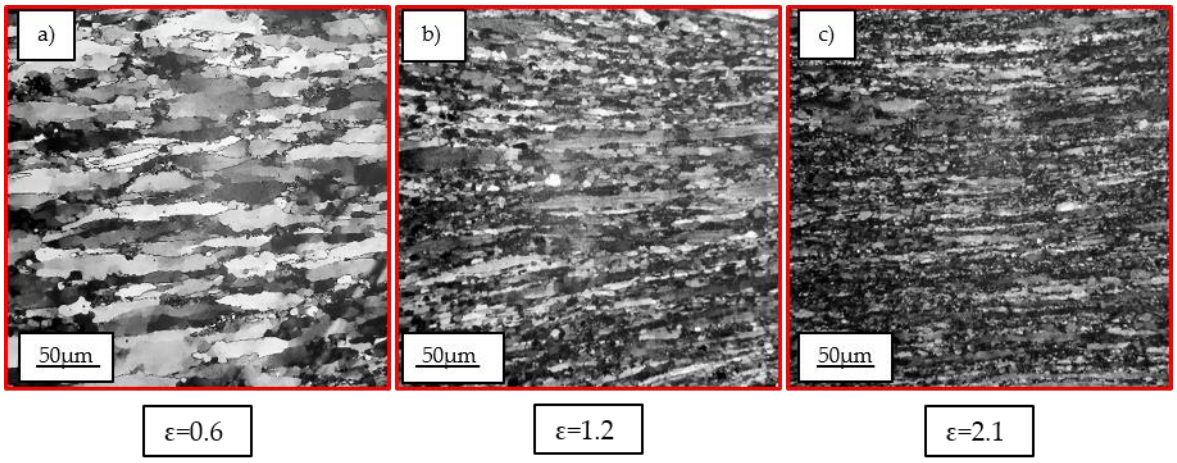

Figure 17:Microstructures of AA7075 at different equivalent strains (temperature 500 °C and strain rate 0.1 s−1): (a) Strain 0.6; (b) Strain 1.2; (c) Strain 2.1.

Further increasing the strain to 1.2, Figure 17 (b), both the serrated grain boundaries and low angle boundaries (LABs) increases. Some new fine recrystallized grains have been formed in the microstructure. And It is observed in both inside the grains and along the Grain Boundaries (GBs), suggesting the occurrence of a mixture of CDRX and DDRX.

When the strain exceeds the critical strain 2.1, Figure 17 (c), the pinching forms the equiaxed grains with HAGBs off serrations in the shear direction indicates GDRX and CDRX). The average grain size of the DRX grains was about 14μm. As a result, a greater number of finer grains can be observed mainly due to the CDRX when the strain is increased. The above analysis shows that several different dynamic recrystallization mechanisms occurred under different deformation conditions.

3.2.3. Deformation feature of hot shear compression specimen

The shear response of alloy AA7075 in the notch section of the specimen at different positions is given by macro and micro images shown in Figure 17. The shear band is observed at 45° to the initial grain structure. From Figure 18 (a) and (c), the buckling (edge effect) is clearly seen at the end of the notches, where the grains are rotated and deformed in various directions. It means that uniform shear strain does not occur at the end section of the notch. Besides, the void nucleation and cracking along the grain boundaries are observed at the end of notches. On the other hand, Figure 18 (b) indicates that the homogeneous deformation is mainly

concentrated in the central part of the notch section and that grains are deformed in the direction of shear loading. This analysis at the microstructural level concludes that optimal specimen geometry and correct design of the test conditions provide the good quality of the shear deformation data.

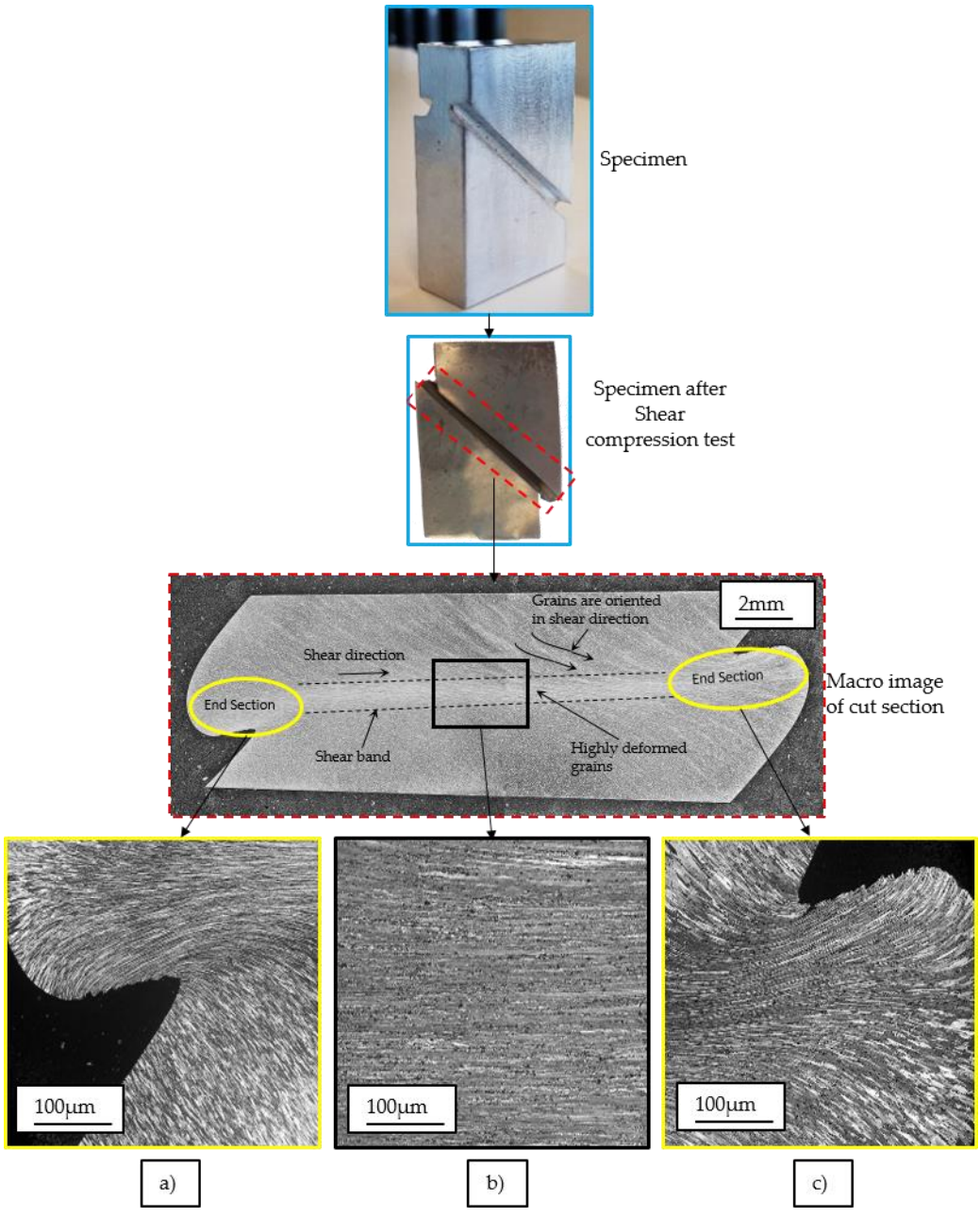

Figure 18:The shear response of alloy AA7075 at different positions of the notch section given by the macro and micro images at 500 °C with an equivalent strain of 2.1 is given by a), b), and c).

Furthermore, the mixture microstructure at the end section of the notch and the microstructure in the thermal mechanically affected zone (TMAZ) of friction stir welding joints show many similarities in grain structure [44]. In addition, the central part of the notch section

looks like the shear bands in the chip formation during machining [45]. The similarities observed between the behavior of the microstructure in the hot shear compression test specimen and the microstructure in different manufacturing processes such as friction welding, machining, etc., the hot shear compression test can be used as a tool which provides a new way to replicate the hot deformation processes to study the adiabatic shear band. It is also possible to determine whether the microstructure is similar to that of the hot shear compression test at different loading conditions. Therefore, further microstructure studies will be necessary for the future.

4. Conclusions

In this paper, the test procedure is developed to study the experimental behavior of the AA7075 alloy over a wide range of temperatures (20°C -500°C) under shear loading using a traditional compression test device, and the following conclusions are drawn.

1. Based on the geometries found in the literature for the shear compression test, a modified shear specimen geometry is designed using FE simulation. The optimized specimen size shows the right aggregate for large deformation and for high temperature avoiding edge effect. It can therefore be concluded that imperfections in the specimen geometry have a major influence on the shear strain data. Hence, it can be concluded that the imperfections in specimen geometry have a major influence on the shear strain data.
2. The new shear specimen shows the uniform distributions of the effective strain in the shear region with less edge effect. The level of shear strain and the equivalent strain was controlled through adjustment of the total height reduction of the specimen and allows to the deformed specimen at large deformation.
3. The microstructure analysis shows that the grains are elongated extensively due to large shear deformation in the notch section. However, at temperatures above 300 °C, new recrystallized grains are formed in the grain boundary. And as the temperature rises,

more and more fine grains are accumulated. The microstructure evolution refers to the mechanism of CDRX with the discontinuous and geometric feature.

4. The macro and micro images show that the grains are uniformly deformed along the direction of the shear load in the central part of the notch. While at the end of the notch, the grains are oriented and deformed in several directions due to the edge effect.

In short, the new shear compression specimen geometry provides a new way to simulate the large plastic deformation at high temperatures. Thus, this type of experimental tests can be used as a tool to develop a material's constitutive equation.

Funding: This project received funding from the European Union's Marie Skłodowska–Curie Actions (MSCA) Innovative Training Networks (ITN) H2020-MSCA-ITN-2017 under the grant agreement N◦764979.

Acknowledgments: The authors want to thanks to David Villalta for helping in experimental setup and Unai Echeveste Elizalde for the help during the metallographic preparation and etching of the samples.

Conflicts of Interest: The authors declare no conflict of interest.

5. References

[1] V. Tarigopula *et al., A study of large plastic deformations in dual phase steel using digital image correlation and FE analysis*, vol. 48, no. 2. 2008.

[2] A. Rusinek and J. . Klepaczko, "Shear testing of a sheet steel at wide range of strain rates and a constitutive relation with strain-rate and temperature dependence of the flow stress," *Int. J. Plast.*, vol. 17, no. 1, pp. 87–115, Jan. 2001, doi: 10.1016/S0749-6419(00)00020-6.

[3] B. B. Hundy and A. P. Green, "A determination of plastic stress-strain relations," *J. Mech. Phys. Solids*, vol. 3, no. 1, pp. 16–21, Oct. 1954, doi: 10.1016/0022-5096(54)90035-6.

[4] L. Murr, *Metallurgical Applications of Shock-Wave and High-Strain-Rate Phenomena*, no. October. 1986.

[5] J. D. Campbell and W. G. Ferguson, "The temperature and strain-rate dependence of the shear strength of mild steel," *Philos. Mag.*, vol. 21, no. 169, pp. 63–82, 1970, doi: 10.1080/14786437008238397.

[6] Z. Wei, J. Yu, J. Li, Y. Li, and S. Hu, "Influence of stress condition on adiabatic shear localization of tungsten heavy alloys," *Int. J. Impact Eng.*, vol. 26, no. 1–10, pp. 843–852, Dec. 2001, doi: 10.1016/S0734-743X(01)00137-3.

[7] G. T. Gray, K. S. Vecchio, and V. Livescu, "Compact forced simple-shear sample for studying shear localization in materials," *Acta Mater.*, 2016, doi: 10.1016/j.actamat.2015.09.051.

[8] D.-K. Kim, S. Lee, and W. Hyung Baek, "Microstructural study of adiabatic shear bands formed by high-speed impact in a tungsten heavy alloy penetrator," 1998.

[9] R. W. Klopp, R. J. Clifton, and T. G. Shawki, "Pressure-shear impact and the dynamic viscoplastic response of metals," *Mech. Mater.*, vol. 4, no. 3–4, pp. 375–385, 1985, doi: 10.1016/0167-6636(85)90033-X.

[10] B. Dodd and Y. Bai, *Adiabatic Shear Localization*. Elsevier, 2012, https://doi.org/10.1016/C2011-0-06979-X.

[11] J. Peirs, P. Verleysen, and J. Degrieck, "Novel Technique for Static and Dynamic Shear Testing of Ti6Al4V Sheet," *Exp. Mech.*, vol. 52, no. 7, pp. 729–741, 2012, doi: 10.1007/s11340-011-9541-9.

[12] A. Brosius, Q. Yin, A. Güner, and A. E. Tekkaya, "A new shear test for sheet metal characterization," *Steel Res. Int.*, vol. 82, no. 4, pp. 323–328, Apr. 2011, doi:

10.1002/srin.201000163.

[13] M. Isakov, J. Seidt, K. O¨stman, A. Gilat, and V.-T. Kuokkala, “Characterization of a Ferritic Stainless Sheet Steel in Simple Shear and Uniaxial Tension at Different Strain Rates,” in *Volume 8: Mechanics of Solids, Structures and Fluids; Vibration, Acoustics and Wave Propagation*, Jan. 2011, pp. 101–109, doi: 10.1115/IMECE2011-63141.

[14] D. Rittel, S. Lee, and G. Ravichandran, “A shear-compression specimen for large strain testing,” *Exp. Mech.*, vol. 42, no. 1, pp. 58–64, 2002, doi: 10.1007/bf02411052.

[15] A. Dorogoy, D. Rittel, and A. Godinger, “A Shear-Tension Specimen for Large Strain Testing,” *Exp. Mech.*, vol. 56, no. 3, pp. 437–449, 2016, doi: 10.1007/s11340-015-0106-1.

[16] S. Moemeni, A. Zarei-Hanzaki, H. R. Abedi, and V. Torabinejad, “The Application of Shear Compression Specimen to Study Shear Deformation Behavior of AZ31 Mg Alloy at High Temperatures and Quasi-Static Regime,” *Exp. Mech.*, vol. 52, no. 6, pp. 629–636, 2012, doi: 10.1007/s11340-011-9525-9.

[17] S. Bouvier, H. Haddadi, P. Levée, and C. Teodosiu, “Simple shear tests: Experimental techniques and characterization of the plastic anisotropy of rolled sheets at large strains,” *J. Mater. Process. Technol.*, vol. 172, no. 1, pp. 96–103, Feb. 2006, doi: 10.1016/j.jmatprotec.2005.09.003.

[18] P. Chwalik, J. R. Klepaczko, and A. Rusinek, “Impact shear-numerical analyses of ASB evolution and failure for Ti-6Al-4V alloy,” *J. Phys. IV JP*, pp. 257–262, 2003, doi: https://doi.org/10.1051/jp4:20020703.

[19] M. R. Rokni, A. Zarei-Hanzaki, A. A. Roostaei, and H. R. Abedi, “An investigation into the hot deformation characteristics of 7075 aluminum alloy,” *Mater. Des.*, vol. 32, no. 4, pp. 2339–2344, 2011, doi: 10.1016/j.matdes.2010.12.047.

[20] T. C. Joshi, U. Prakash, and V. V. Dabhade, “Microstructural development during hot forging of Al 7075 powder,” *J. Alloys Compd.*, vol. 639, no. March, pp. 123–130, 2015, doi: 10.1016/j.jallcom.2015.03.099.

[21] W. Xiao, B. Wang, Y. Wu, and X. Yang, “Constitutive modeling of flow behavior and microstructure evolution of AA7075 in hot tensile deformation,” *Mater. Sci. Eng. A*, vol. 712, pp. 704–713, 2018, doi: 10.1016/j.msea.2017.12.028.

[22] X. Yang, H. Miura, and T. Sakai, “Continuous dynamic recrystallization in a superplastic 7075 aluminum alloy,” *Mater. Trans.*, vol. 43, no. 10, pp. 2400–2407, 2002, doi: 10.2320/matertrans.43.2400.

[23] Engineering ToolBox, “Friction and Friction Coefficients,” 2004. https://www.engineeringtoolbox.com/friction-coefficients-d_778.html.

[24] J. O. Hallquist, “LS-DYNA ® THEORY MANUAL,” 2006. [Online]. Available: www.lstc.com.

[25] R. W. Armstrong and F. J. Zerilli, “Dislocation mechanics based analysis of material dynamics behavior,” *Le J. Phys. Colloq.*, vol. 49, no. C3, pp. C3-529-C3-534, Sep. 1988, doi: 10.1051/jphyscol:1988374.

[26] D. J. Steinberg, S. G. Cochran, and M. W. Guinan, “A constitutive model for metals applicable at high-strain rate,” *J. Appl. Phys.*, vol. 51, no. 3, pp. 1498–1504, 1980, doi: 10.1063/1.327799.

[27] R. F. Muraca and J. S. Whittick, “Aluminum Alloy 7075 (2nd Edition),” in *Materials Data Handbook*, San Carlos, California, 1972, p. 132.

[28] ASM matweb, “Aluminum 7075-T6; 7075-T651,” 2018. http://asm.matweb.com/search/SpecificMaterial.asp?bassnum=MA7075T6.

[29] N. S. Brar, V. S. Joshi, and B. W. Harris, “Constitutive model constants for Al7075-T651 and Al7075-T6,” *AIP Conf. Proc.*, vol. 1195, no. 1, pp. 945–948, 2009, doi: 10.1063/1.3295300.

[30] D. N. Zhang, Q. Q. Shangguan, C. J. Xie, and F. Liu, “A modified Johnson-Cook model of dynamic tensile behaviors for 7075-T6 aluminum alloy,” *J. Alloys Compd.*, vol. 619, pp. 186–194, 2015, doi: 10.1016/j.jallcom.2014.09.002.

[31] G. E. Dieter, H. a. Kuhn, and S. L. Semiatin, “Handbook of Workability and Process Design,” *Handb. Work. Process Des.*, pp. 278–290, 2003, doi: 10.1361/hwpd2003p232.

[32] J.-H. Ouyang and X.-S. Liang, “High-Temperature Solid Lubricating Materials,” *Encycl. Tribol.*, pp. 1671–1681, 2013, doi: 10.1007/978-0-387-92897-5_1236.

[33] Y. Li, K. T. Ramesh, and E. S. C. Chin, “The mechanical response of an A359/SiCp MMC and the A359 aluminum matrix to dynamic shearing deformations,” *Mater. Sci. Eng. A*, vol. 382, no. 1–2, pp. 162–170, Sep. 2004, doi: 10.1016/j.msea.2004.04.062.

[34] A. Dorogoy, D. Rittel, and A. Godinger, “Modification of the Shear-Compression Specimen for Large Strain Testing,” *Exp. Mech.*, vol. 55, no. 9, pp. 1627–1639, 2015, doi: 10.1007/s11340-015-0057-6.

[35] R.J. Clifton and R.W. Klopp: Metals Handbook, 9th ed., ASM INTERNATIONAL, Metals Park, OH, 1986, vol. 8, p. 230.

[36] R. K. GUPTA, C. Mathew, and P. Ramkumar, “Strain Hardening in Aerospace Alloys,” *Front. Aerosp. Eng.*, vol. 4, no. 1, pp. 1–13, 2015, doi: 10.12783/fae.2015.0401.01.

[37] S. Gourdet and F. Montheillet, “A model of continuous dynamic recrystallization,” *Acta Mater.*, vol. 51, no. 9, pp. 2685–2699, May 2003, doi: 10.1016/S1359-6454(03)00078-8.

[38] W. H. Van Geertruyden, W. Z. Misiolek, and P. T. Wang, “Grain structure evolution in a 6061 aluminum alloy during hot torsion,” *Mater. Sci. Eng. A*, vol. 419, no. 1–2, pp. 105–114, 2006, doi: 10.1016/j.msea.2005.12.018.

[39] Z. C. Sun, L. S. Zheng, and H. Yang, “Softening mechanism and microstructure evolution of as-extruded 7075 aluminum alloy during hot deformation,” *Mater. Charact.*, vol. 90, pp. 71–80, 2014, doi: 10.1016/j.matchar.2014.01.019.

[40] T. M. Yue, L. J. Yan, C. P. Chan, C. F. Dong, H. C. Man, and G. K. H. Pang, “Excimer laser surface treatment of aluminum alloy AA7075 to improve corrosion resistance,” *Surf. Coatings Technol.*, vol. 179, no. 2–3, pp. 158–164, 2004, doi: 10.1016/S0257-8972(03)00850-8.

[41] S. C. Jacumasso, J. de P. Martins, and A. L. M. de Carvalho, “Analysis of precipitate density of an aluminium alloy by TEM and AFM,” *Rev. Esc. Minas*, vol. 69, no. 4, pp. 451–457, 2016, doi: 10.1590/0370-44672016690019.

[42] H. V. Atkinson, K. Burke, and G. Vaneetveld, “Recrystallization in the semi-solid state in 7075 aluminium alloy,” *Mater. Sci. Eng. A*, vol. 490, no. 1–2, pp. 266–276, 2008, doi: 10.1016/j.msea.2008.01.057.

[43] T. Sakai, A. Belyakov, R. Kaibyshev, H. Miura, and J. J. Jonas, “Dynamic and post-dynamic recrystallization under hot, cold and severe plastic deformation conditions,” *Prog. Mater. Sci.*, vol. 60, no. 1, pp. 130–207, 2014, doi: 10.1016/j.pmatsci.2013.09.002.

[44] L. Jing, R. D. Fu, Y. J. Li, Y. Shi, J. Wang, and D. X. Du, “Physical simulation of microstructural evolution in linear friction welded joints of Ti – 6Al – 4V alloy,” *Sci. Technol. Weld. Join.*, vol. 20, no. 4, pp. 286–290, 2015, doi: 10.1179/1362171815Y.0000000007.

[45] P. Longère and A. Dragon, “Dynamic vs. quasi-static shear failure of high strength

metallic alloys: Experimental issues," *Mech. Mater.*, vol. 80, no. PB, pp. 203–218, 2015, doi: 10.1016/j.mechmat.2014.05.001.